Astronomy & Astrophysics manuscript no. paper
December 12, 2008

Benchmarking atomic data for astrophysics

Fe XVII EUV lines

G. Del Zanna[1], Y. Ishikawa[2], and E. Traébert[3]

[1] DAMTP, Centre for Mathematical Sciences, Wilberforce road Cambridge CB3 0WA UK

[2] Department of Chemistry, University of Puerto Rico, P.O. Box 23346, San Juan, PR 00931-3346, USA

[3] Astronomisches Institut, Ruhr-Universitat Bochum, D-44780 Bochum, Germany;
High Temperature and Astrophysics Division, LLNL, P.O. Box 808, Livermore, CA 94550, USA

Received ; accepted

ABSTRACT

We review, in light of accurate structure and scattering calculations for Fe XVII, the status of the identifications in the EUV lines of this ion. Most previous identifications are confirmed, however wavelengths are critically revised. A few new transitions are identified in Hinode/EIS spectra of solar flares.

Key words. Atomic data – Line: identification – Sun: flares – Techniques: spectroscopic

1. Introduction

This paper is one of a series in which atomic data and line idetifications are benchmarked against experimental data.

Fe XVII produces many 3s-3p and 3p-3d transitions that fall at EUV wavelengths, with contradicting identifications found in the literature.

Most previous identifications came from observations of solar flares with the Skylab NRL slitless spectrograph, which observed the 171-630 Å range. Recently, there is a large interest in the solar physics community in Fe XVII lines, considering that some of them are observed with the Hinode EUV Imaging Spectrometer (EIS, see Culhane et al. 2007), which covers two wavelength bands (SW: 163–209 Å; LW: 242–289 Å). This instrument allows accurate measurements of line intensities and wavelengths. Del Zanna (2008) provided a preliminary assesment of the most prominent lines formed at high temperatures in the EIS spectra and confirmed the identifications of the brightest Fe XVII lines, with one new identification.

The new R-matrix atomic calculations of Loch et al. (2006) predict Fe XVII line intensities that are largely different (factors of 2–3) from previous estimates. The aim of this paper is to support these accurate scattering calculations with new relativistic multireference many-body perturbation theory calculations, reassess previous identifications, and suggest which lines are best for diagnostic purposes.

2. Previous identifications

The identification of Fe XVII lines started with the excellent (basically unsurpassed) work of Tyrén (1938).

Here, we are concerned with the $2p^5$ 3s - $2p^5$ 3p and $2p^5$ 3p - $2p^5$ 3d EUV transitions, however all previous measurements for the X-ray and UV lines had to be assessed. This assesment is presented in a separate paper, where the X-ray lines are benchmarked.

The Skylab NRL slitless spectrograph produced spectra of flares in the 171-630 Å range, which allowed a number of identifications to be made (cf. Sandlin et al. 1976 and Dere 1978). It was however the work along the isoelectronic sequence which allowed Jupen (1984) to suggest a more complete list of identifications in the Skylab spectra. Readers should note that Jupen (1984) provided labelling of levels based on the LS coupling of ions in the lower part of the sequence. This is very much different from the correct labeling which takes into account level mixing. The key to interpret the Jupen (1984) identifications is actually in the energies listed in Jupén & Litzén (1984). Soon after, Feldman et al. (1985) considered Skylab spectra in the 290-410 Å range and revised a number of identifications proposed by Jupen (1984). Their work was based on studying the morphology of the lines, and on the calculations available at the time (Bhatia et al. 1985). The labelling of levels in Feldman et al. (1985) follows the conventions used in Jupén & Litzén (1984), but the identifications are actually based on the structure calculation presented in Bhatia et al. (1985), which also did a distorted-wave calculation and provided estimated line intensities, which were used by Feldman et al. (1985) as an aid in the identification. These line intensities are listed within Table 1, to show how different they are, compared to those based on the recent calculations.

Almost at the same time, Buchet et al. (1985) published a list of identifications of lines in their laboratory spectra. Their observtions signifcantly differ from the solar ones in that the prominent lines there are not the same. Wavelengths were not very accurate.

3. Results

Relativistic multireference many-body perturbation theory calculations (hereafter referred to as MR-MP) were performed along the Ne-like sequence. State-averaged multiconfiguration Dirac-Fock-Breit self-consistent field (MCDFB SCF) +multireference configuration interaction (MR-CI) calculations are followed by a state-specific multireference Moller- Plesset (MR-MP) perturbation treatment. This yields highly accurate term and level energies. For details of the procedure see, e.g. Ishikawa & Vilkas (2008).

Line intensities were calculated with the rates and transition probabilities provided by Loch et al. (2006), at the temperature of peak ion abundance for Fe XVII in ionization equilibrium (log T[K] = 6.6). Table 1 shows relative line intensities calculated in the low-density regime (but still at densities typical for solar flares) and in the high-density one. Lines are ordered with their intensities. It is very satisfactory to see that all the brightest lines have now been observed.

Table 2 lists the identifications and wavelength measurements used to obtain the level energies. Whenever available, we used the accurate measurements from Thomas & Neupert (1994) or those obtained here from Hinode/EIS.

Wavelengths obtained from the energies of the MR-MP are also shown in Table 1, together with those from NIST. Table 1 clearly shows an excellent agrement between the MR-MP wavelengths

and the measured ones, the only notable exception being the two decays from the 3p $^1S_0$ level. Indeed the MR-MP wavelengths have been used to look for further weaker lines.

Line intensities, whenever available, were compared, in order to confirm identifications and assess for the presence of blending. This was done with the use of the 'emissivity ratio' technique, whereby the observed intensity of a line is divided by its emissivity (as a function of density in this paper). This allows in one single plot to assess how good observed vs. theoretical intensities are for a group of lines at once.

The first check was done on the EUV lines in the longer wavelengths, observed by Skylab. Fig. 1 shows the results based on the measurements of Doschek et al. (1991). The comparison is satisfactory. The lines observed at 254.53, 269.88, 266.42, 275.55Å appear to have been significantly blended. Most other lines agree to within the stated 30% uncertainty, with the exception of the lines observed at 351.55, 358.24, 409.69 Å, which are a factor of 2 too weak. These lines are quite weak so it is possible that the problem was in the measurement.

The second check was done with the intensities observed during the SERTS-89 rocket flight (Thomas & Neupert 1994). Intensities are weak since the instrument observed a non-flaring active region. Here, the observations suggest that the 254.88 and 389.11 Å lines are significantly blended. The 389.11 Å line ha a known blend with Ar XVI, but the former is puzzling.

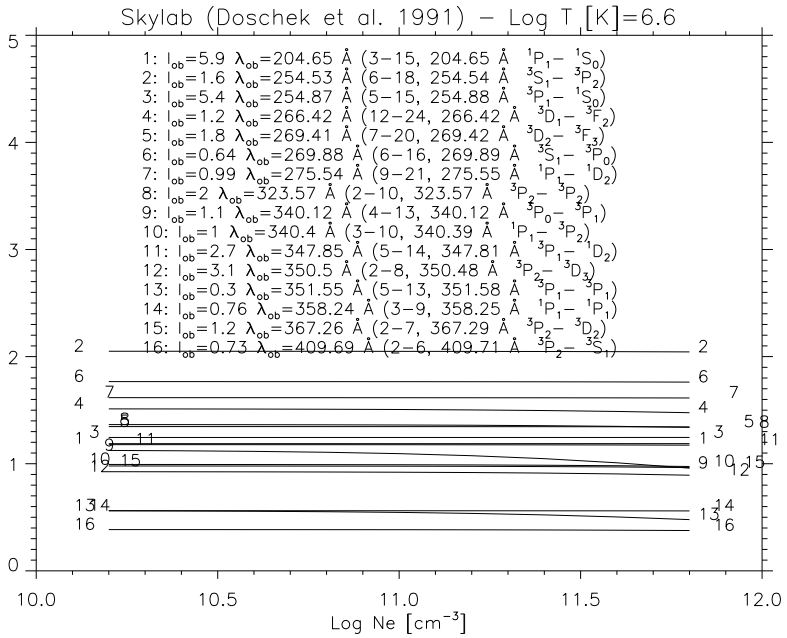

Fig. 1. The emissivity ratio curves (at log T[K]=6.6) relative to the transitions observed by the Skylab NRL spectrometer during a flare (Doschek et al. 1991).

3.1. Hinode/EIS data

The same observation presented by Del Zanna (2008) has been reanalysed here. It consisted of a full spectral atlas over AR 10960, where the 1″slit was moved (from West to East) on June 2nd 2007, and recorded a B2-class flare which occurred between 20:32 and 20:38 UT. As described in Del Zanna (2008), the main problems in the analysis of EIS data are the strong (75 km/s) or-

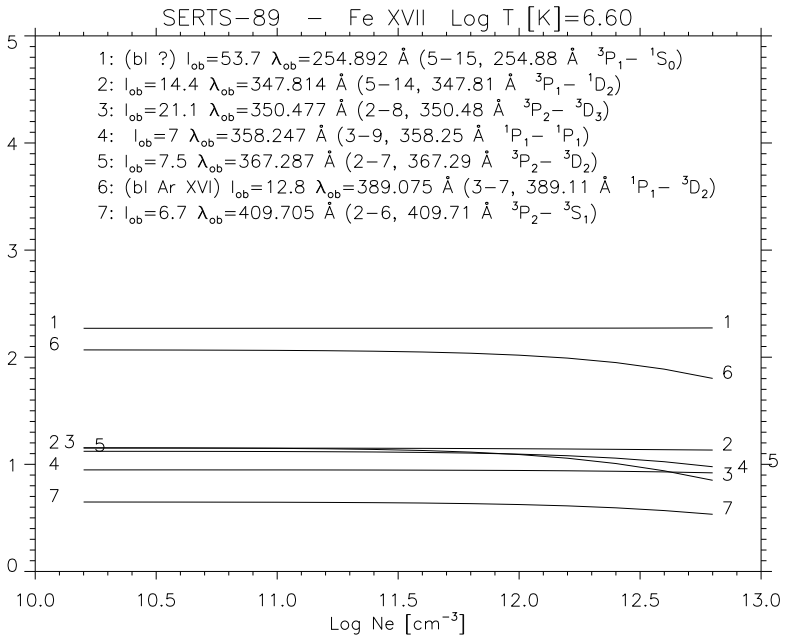

Fig. 2. The emissivity ratio curves (at log T[K]=6.6) relative to the transitions observed on an active region during the 1989 SERTS rocket flight (Thomas & Neupert 1994).

bital variation of the wavelength scale, and the offsets in both N-S (18″) and E-W (2″) directions between the two channels. The offset in the E-W direction means that observations in the two channels are not simultaneous nor co-spatial. The reanalysis done here differed from the previous one in many respects. Treatment of 'warm', 'hot' and 'dust' pixels is now included, as well as a full wavelength calibration. A further significant effect which was found during the course of this work is a slant of the spectra relative to the axes of the CCD. The intensities of lines emitted by the same ion within each channel were cross-correlated to look for possible misalignements. This was non-trivial, as very few pairs of lines were found. In the LW channel, the strong Fe XVII lines at 254.9,269.4,281.2Å were used. However, all measurements consistently indicate the presence of a linear slant in both channels, equivalent to a displacement in the N-S direction (along the slit) of about 3.66(±0.2) pixels end-to-end (each pixel along the slit corresponds to 1″). This slant need to be taken into account when comparing intensities from lines which are not very close in wavelength, and in particular for a case such as this one, where flare lines can have a drop in intensity of an order of magnitude within 2-3 pixels. The slant has been corrected by rotating the spectra. Another issue is line broadening and blending. The location of brightest Fe XVII emission which was considered in Del Zanna (2008) is an area where lines are broadened and very strong cooler emission is present. For this study, averaged spectra were obtained from three consecutive exposures in locations where the Fe XVII emission was less affected by blending. These averaged spectra are shown in Fig. 3.1. The averaged spectra were calibrated in wavelength, using a set of about 30 lines in each channel. Although an EIS linear wavelength calibration fits the observations very well, a quadratic one was used here (differences are of the order of 2-3 mÅ). Theoretical wavelengths as in the version 5.2 of the CHIANTI atomic package (Landi et al. 2006) were used. It is well known that theoretical wavelengths need to be improved, and indeed this is one of the by-products of the on-going benchmark work. Overall, as Fig. 3.1 shows, the EIS spectra provide wavelengths

accurate to within 5 mÅ across the entire spectral range, although a conservative uncertainty of 10 mÅ is adopted here.

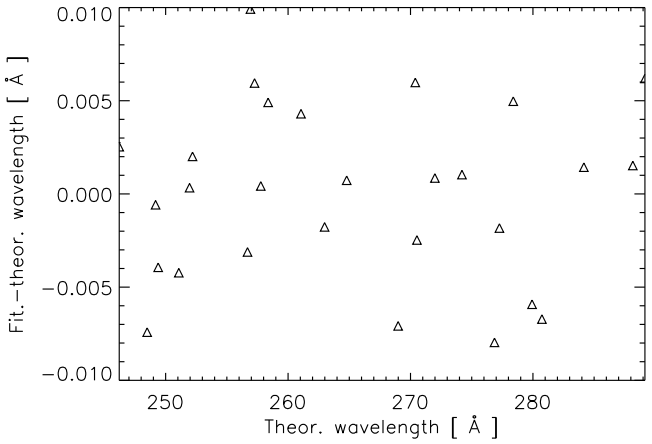

Fig. 3. Difference between observed and theoretical wavelengths (Å) in the LW channel, after a quadratic calibration was applied to the spectrum.

Fig. 5 shows the emissivity ratio curves for this observation. Most lines agree within 20%. The 269.89 is confirmed to be significantly blended (more than 50%). The weaker 259.71,262.70, 273.35, and 279.24 Å, all identified here for the first time, also apper to be significantly blended. The line observed at 283.945 Å and identified here for the first time is in good agreement, considering that its intensitiy is very difficult to measure, being close to an Al IX and in the wings of the strong Fe XV 284.1Å line. Note that all the newly identified lines show a similar morphology as the other Fe XVII lines.

The 204.668 Å is in good agreement with the other lines, despite the lack of simultaneity in the observations. The main puzzle is the intensity of the 254.88 Å, which is, as already mentioned in Del Zanna (2008), weaker by more than 50%, compared to prediction. The puzzling aspect is the fact that these two lines share the same upper level (branching ratio), and their ratio must be close to one. Their morphology clearly indicates that these two strong lines must either be due to Fe XVII or an ion formed at the same temperature. There are no other strong lines within a few Å and the same morphology, so these two lines must be correctly identified. We provide here a new wavelength of 254.885 Å, which, combined with energies of the $3s\ ^3, 1P_1$ obtained from the X-ray lines, provides a wavelength of 204.652 Å, in good agreement with the observed 204.668 Å.

We have checked branching ratios and other good line ratios across the LW channel to see if the radiometric calibration could be at fault, but did not find significant problems yet, so a problem in the calibration is to be excluded.

Many other Hinode/EIS observations have been analysed, to confirm the present results. In general, we found many instances where most of the Fe XVII lines are actually blended with unidentified lines, in one place or the other. Most notably with the 204.66 Å line. This becomes more evident when Fe XVII intensities become even weaker.

Another observation where Fe XVII lines are significantly bright gives results consistent to those presented here.

Table 1. Line details. The relative intensities (photons) $Int = N_j A_{ji}/N_e$ are normalised to te strongest transition and were calculated at densities of 10^{11} and 10^{19}. The fifth column provides the relative intensities calculated by Bhatia et al. (1985) as reported in Feldman et al. (1985). gf and A-values as in Loch et al. (2006) are reported. λ_{best} are our best estimated wavelengths, λ_{CC} are those from the scattering calculation (Loch et al. 2006), while λ_{NIST} are those from NIST v.3 and λ_{MR-MP} are those obtained from the MR-MP calculations.

i-j	Transition	*Int*	*Int*	*Int*(B84)	gf	$A_{ji}(s^{-1})$	λ_{best}	λ_{CC}	λ_{NIST}	λ_{MR-MP}
		$1.0\ 10^{11}$	$1.0\ 10^{19}$							
3-15	3s $^1P_1$–3p $^1S_0$	1.0	0.23	1	$8.0\ 10^{-2}$	$1.4\ 10^{10}$	204.652	196.38	204.650	205.34
5-15	3s $^3P_1$–3p $^1S_0$	1.1	0.25	1.1	0.13	$1.5\ 10^{10}$	254.885	243.47	254.751	255.93
2-8	3s $^3P_2$–3p $^3D_3$	1.2	0.62	0.54	0.82	$6.5\ 10^{9}$	350.478	348.22	350.582	350.30
5-14	3s $^3P_1$–3p $^1D_2$	0.78	0.19	0.28	0.60	$6.6\ 10^{9}$	347.814	345.98	347.959	347.69
2-6	3s $^3P_2$–3p $^3S_1$	0.77	0.13	0.4	0.26	$3.4\ 10^{9}$	409.705	408.70	409.903	409.30
8-19	3p $^3D_3$–3d $^3F_4$	0.42	0.93	0.27	1.23	$1.1\ 10^{10}$	283.942	282.86	284.010	283.97
2-10	3s $^3P_2$–3p $^3P_2$	0.47	0.23	0.17	0.35	$4.6\ 10^{9}$	323.572	321.97	323.646	323.50
3-9	3s $^1P_1$–3p $^1P_1$	0.48	0.11	0.16	0.33	$5.7\ 10^{9}$	358.247	356.33	358.320	358.05
7-20	3p $^3D_2$–3d $^3F_3$	0.35	0.57	0.16	0.85	$1.1\ 10^{10}$	269.420	267.82	269.295	269.44
14-26	3p $^1D_2$–3d $^1F_3$	0.37	0.39	0.14	0.98	$1.2\ 10^{10}$	280.160	278.64	280.198	280.24
2-7	3s $^3P_2$–3p $^3D_2$	0.44	0.13	0.18	0.26	$2.6\ 10^{9}$	367.288	365.48	367.377	367.16
3-7	3s $^1P_1$–3p $^3D_2$	0.44	0.13	0.17	0.29	$2.6\ 10^{9}$	389.111	387.50	389.226	388.93
10-22	3p $^3P_2$–3d $^3D_3$	0.29	0.51	0.092	0.81	$1.0\ 10^{10}$	280.160	278.32	280.206	280.17
3-10	3s $^1P_1$–3p $^3P_2$	0.34	0.16	0.14	0.28	$3.3\ 10^{9}$	340.391	338.93	340.483	340.28
4-13	3s $^3P_0$–3p $^3P_1$	0.34	$9.6\ 10^{-2}$	0.13	0.21	$4.1\ 10^{9}$	340.124	338.42	340.136	339.97
3-11	3s $^1P_1$–3p $^3P_0$	0.27	$3.6\ 10^{-2}$	0.1	0.10	$8.0\ 10^{9}$	295.981	293.43	296.314	295.77
13-25	3p $^3P_1$–3d $^3D_2$	0.24	0.28	0.14	0.59	$1.0\ 10^{10}$	281.120	279.65	281.104	281.16
12-24	3p $^3D_1$–3d $^3F_2$	0.21	0.28	0.11	0.62	$1.2\ 10^{10}$	266.417	265.20	266.432	266.45
6-18	3p $^3S_1$–3d $^3P_2$	0.20	0.22	0.13	0.27	$5.5\ 10^{9}$	254.536	253.32	254.485	254.60
5-12	3s $^3P_1$–3p $^3D_1$	0.29	$5.6\ 10^{-2}$	0.11	0.19	$2.8\ 10^{9}$	387.237	385.26	387.357	387.02
9-21	3p $^1P_1$–3d $^1D_2$	0.17	0.23	0.067	0.46	$8.1\ 10^{9}$	275.550	274.28	275.596	275.60
4-12	3s $^3P_0$–3p $^3D_1$	0.22	$4.2\ 10^{-2}$	0.084	0.13	$2.1\ 10^{9}$	373.385	370.93	373.385	373.25
5-13	3s $^3P_1$–3p $^3P_1$	0.19	$5.5\ 10^{-2}$	0.074	0.13	$2.3\ 10^{9}$	351.580	350.31	351.692	351.36
10-18	3p $^3P_2$–3d $^3P_2$	0.13	0.15	0.098	0.26	$3.8\ 10^{9}$	304.971	304.09	304.943	304.91
7-21	3p $^3D_2$–3d $^1D_2$	0.10	0.14	0.039	0.25	$5.1\ 10^{9}$	259.705	258.29	259.734	259.72
6-16	3p $^3S_1$–3d $^3P_0$	$9.6\ 10^{-2}$	0.10	0.072	0.12	$1.1\ 10^{10}$	269.886	269.62	269.884	269.98
8-22	3p $^3D_3$–3d $^3D_3$	$7.9\ 10^{-2}$	0.14	-	0.20	$2.7\ 10^{9}$	262.699	261.29	262.729	262.76
2-13	3s $^3P_2$–3p $^3P_1$	$7.2\ 10^{-2}$	$2.1\ 10^{-2}$	-	$2.5\ 10^{-2}$	$8.9\ 10^{8}$	252.525	250.31	252.704	252.44
8-20	3p $^3D_3$–3d $^3F_3$	$5.8\ 10^{-2}$	$9.3\ 10^{-2}$	-	0.15	$1.8\ 10^{9}$	279.245	277.91	279.096	279.31
33-37	3p $^1P_1$–3d $^1D_2$	$4.9\ 10^{-2}$	$4.9\ 10^{-2}$	-	0.71	$1.3\ 10^{10}$	273.347	271.73	-	273.52
9-18	3p $^1P_1$–3d $^3P_2$	$3.6\ 10^{-2}$	$4.0\ 10^{-2}$	-	$6.5\ 10^{-2}$	$1.0\ 10^{9}$	291.934	291.33	291.928	291.93
7-18	3p $^3D_2$–3d $^3P_2$	$3.3\ 10^{-2}$	$3.7\ 10^{-2}$	-	$5.3\ 10^{-2}$	$9.4\ 10^{8}$	274.210	273.35	274.190	274.18
6-17	3p $^3S_1$–3d $^3P_1$	$2.8\ 10^{-2}$	$9.3\ 10^{-2}$	-	0.30	$9.7\ 10^{9}$	264.785	263.63	264.306	264.47
14-25	3p $^1D_2$–3d $^3D_2$	$3.0\ 10^{-2}$	$3.5\ 10^{-2}$	-	$7.5\ 10^{-2}$	$1.2\ 10^{9}$	283.575	282.48	283.535	283.56
5-11	3s $^3P_1$–3p $^3P_0$	$4.0\ 10^{-2}$	$5.4\ 10^{-3}$	-	$3.0\ 10^{-2}$	$1.2\ 10^{9}$	413.976	412.69	414.285	413.52
14-24	3p $^1D_2$–3d $^3F_2$	$2.5\ 10^{-2}$	$3.3\ 10^{-2}$	-	$8.7\ 10^{-2}$	$1.4\ 10^{9}$	288.950	287.69	288.934	288.95
2-9	3s $^3P_2$–3p $^1P_1$	$2.8\ 10^{-2}$	$6.4\ 10^{-3}$	-	$1.7\ 10^{-2}$	$3.4\ 10^{8}$	339.666	337.62	339.720	339.51

Fig. 4. Averaged EIS spectrum (units are counts) over an area where Fe XVII was more clearly isolated.

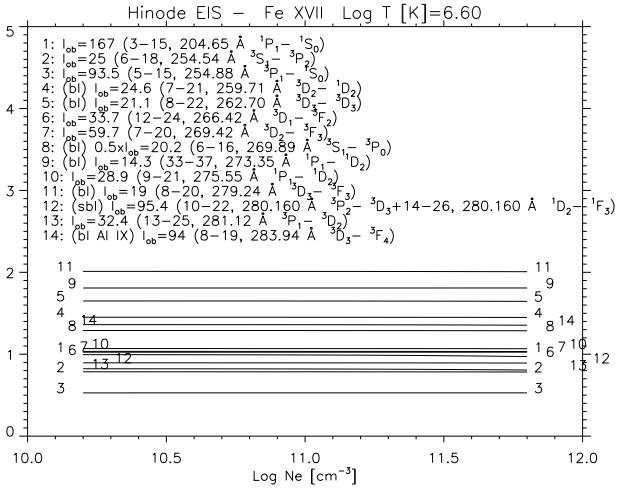

Fig. 5. The emissivity ratio curves (at log T[K]=6.6) relative to the transitions observed during the B-class flare by Hinode/EIS.

4. Conclusions

We have shown that wavelengths based on the MR-MP calculations are in excellent agreement with observations, which gives us confidence in using them to further assess line identifications along the sequence. We have confirmed previous Fe XVII identifications, but revised a significant number of wavelengths. We have identified in Hinode/EIS spectra a few weaker lines not previously observed in solar spectra, although most of them appear to be significantly blended in a very small (B-class) flare. Further observations of larger flares would be needed. Hinode/EIS observations consistently record the 254.885 Å line with an intensity 50% of what it should be.

Acknowledgements. Support from STFC (Advanced Fellowship and APAP network) is acknowledged by GDZ.

Table 2. List of identifications. The relative intensities (photons) $Int = N_j A_{ji}/N_e$ are are calculated at a density of 10^{11} and normalised. D78: Dere (1978); J84: Jupen (1984); F85:Feldman et al. (1985); B85: Buchet et al. (1985); TN94:Thomas & Neupert (1994); F98: Feldman et al. (1998). N indicates a new measurement or identification proposed here. (bl) indicates the presence of a blend. Values in parentheses indicate the uncertainty in the wavelength measurement.

i-j	*Int*	λ_{best}(Å)	$\lambda_{observed}$(Å)	Same ID	Diff. ID	
3-15	1.0	204.652	204.668(10) N (bl ?)	D78		
6-18	0.20	254.536	254.536(10) N (bl)	J84,B85(254.48)		
5-15	1.1	254.885	254.885(10) N (bl Fe XXII)	D78(254.87)		
7-21	0.10	259.705	259.722(10) N (bl)			N
8-22	$7.9\ 10^{-2}$	262.699	262.699(10) N (bl)			N
6-17	$2.8\ 10^{-2}$	264.785	(bl Fe XIV)			N
12-24	0.21	266.417	266.417(10) N	J84,B85(266.43)		
7-20	0.35	269.420	269.420(10) N	J84	?B85(269.61)	
6-16	$9.6\ 10^{-2}$	269.886	269.886(10) N (bl)	J84		
33-37	$4.9\ 10^{-2}$	273.347	273.347(10) N (bl)			N
7-18	$3.3\ 10^{-2}$	274.210	(bl Fe XIV)			N
9-21	0.17	275.550	275.550(10) N	J84,B85(275.60)		
8-20	$5.8\ 10^{-2}$	279.245	279.240(10) N (bl)			N
10-22	0.29	280.160	280.160(10) N (sbl)	J84(280.14),B85, D08		
14-26	0.37	280.160	280.160(10) N (sbl)	D08	J84(279.21),B85(279.1)	
13-25	0.24	281.120	281.120(10) N	J84(281.09), B85		
8-19	0.42	283.942	283.945(10) N	B85(284.01)	J84(284.17)	N
14-24	$2.5\ 10^{-2}$	288.950	288.960(10) weak			N
3-11	0.27	295.981	295.98(2) D78	F85	J84(297.34),B85(297.46)	
10-18	0.13	304.971	304.971(10) (bl) N	B85(304.93 bl)		
2-10	0.47	323.572	323.57(20) D78	J84, B85(323.65 bl)		
4-13	0.34	340.124	340.12(20) D78	F85	J84(337.23)	
3-10	0.34	340.391	340.40(20) D78	J84,B85(340.47)		
5-14	0.78	347.814	347.814(4) TN94	J84	B85(347.96)	
2-8	1.2	350.478	350.477(5) TN94	J84,B85(350.58)		
5-13	0.19	351.580	351.58(20) D78	F85, B85(351.69)		
3-9	0.48	358.247	358.247(6) TN94	J84	?B85	
2-7	0.44	367.288	367.287(8) TN94	F85,B85(367.37 bl)	J84(365.62)	
4-12	0.22	373.385	? 373.41(20) F85	F85	B85(372.93 bl)	
5-12	0.29	387.237	387.23(20) D78	F85, B85(387.36 bl)		
3-7	0.44	389.111	389.11(20) (bl Ar XVI)	F85, B85(389.25)	J84(387.23)	
2-6	0.77	409.705	409.705(6) TN94	F85	J84(410.46) B85(409.91 bl)	
3-4	0.64	1153.16	1153.16(2) F98	F85		

Hinode is a Japanese mission developed and launched by ISAS/JAXA, with NAOJ as domestic partner and NASA and STFC (UK) as international partners. It is operated by these agencies in co-operation with ESA and NSC (Norway).

References

Bhatia, A. K., Feldman, U., & Seely, J. F. 1985, Atomic Data and Nuclear Data Tables, 32, 435

Buchet, J.-P., Buchet-Poulizac, M.-C., Denis, A., et al. 1985, Phys. Scr, 31, 364

Culhane, J. L., Harra, L. K., James, A. M., et al. 2007, Sol. Phys., 60
Del Zanna, G. 2008, A&A, 481, L69
Dere, K. P. 1978, ApJ, 221, 1062
Doschek, G. A., Feldman, U., & Bhatia, A. K. 1991, Phys. Rev. A, 43, 2565
Feldman, U., Curdt, W., Doschek, G. A., et al. 1998, ApJ, 503, 467
Feldman, U., Doschek, G. A., & Seely, J. F. 1985, MNRAS, 212, 41P
Ishikawa, Y. & Vilkas, M. J. 2008, Phys. Rev. A, 78, 042501
Jupen, C. 1984, MNRAS, 208, 1P
Jupén, C. & Litzén, U. 1984, Phys. Scr, 30, 112
Landi, E., Del Zanna, G., Young, P. R., et al. 2006, ApJS, 162, 261
Loch, S. D., Pindzola, M. S., Ballance, C. P., & Griffin, D. C. 2006, Journal of Physics B Atomic Molecular Physics, 39, 85
Sandlin, G. D., Brueckner, G. E., Scherrer, V. E., & Tousey, R. 1976, ApJ, 205, L47
Thomas, R. J. & Neupert, W. M. 1994, ApJS, 91, 461
Tyrén, F. 1938, Zeitschrift fur Physik, 111, 314